THE JOURNAL OF PHYSICAL CHEMISTRY Letters

Letter

pubs.acs.org/JPCL

Simultaneous Observation of an Intraband Transition and Distinct Transient Species in the Infrared Region for Perovskite Solar Cells

Sudhakar Narra,[†] Chih-Chun Chung,[†] Eric Wei-Guang Diau,*[,†] and Shinsuke Shigeto*[,‡]

[†]Department of Applied Chemistry and Institute of Molecular Science, National Chiao Tung University, Hsinchu 30010, Taiwan

[‡]Department of Chemistry, School of Science and Technology, Kwansei Gakuin University, Sanda 669-1337, Japan

Supporting Information

ABSTRACT: Solar cells based on organometal-halide perovskites such as $CH_3NH_3PbI_3$ have emerged as a promising next-generation photovoltaic system, but the underlying photophysics and photochemistry remain to be established because of the limited availability of methods to implement the simultaneous and direct measurement of various charge carriers and ions that play a crucial role in the operating device. We used nanosecond time-resolved infrared (IR) spectroscopy to investigate, with high molecular specificity, distinct transient species that are formed in perovskite solar cells after photoexcitation. In $CH_3NH_3PbI_3$ planar-heterojunction solar cells, we simultaneously observed infrared spectral signatures that are associated with an intraband transition of conduction-band electrons, Fano resonance, and the spiro-OMeTAD cation having an exceptionally short lifetime of 1.0 μs (at ~1485 cm^{-1}). The present results show that the time-resolved IR method offers a unique capability to elucidate these important transients in perovskite solar cells and their dynamic interplay in a comprehensive manner.

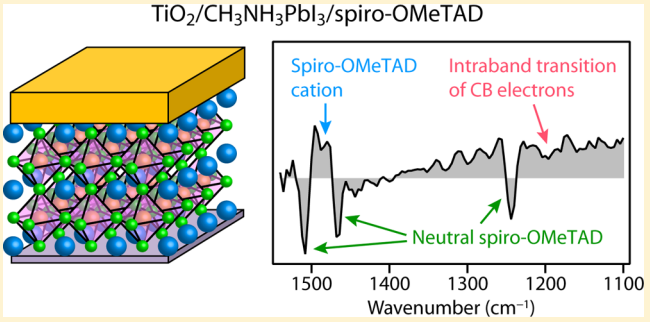

Since 2012, the development of all-solid-state solar cells based on organic–inorganic hybrid lead-halide-perovskite $MAPbX_3$ (MA = $CH_3NH_3^+$; X = Cl^-, Br^-, and/or I^-) semiconductors has surged.[1−10] Perovskite solar cells are easy to fabricate at low cost through solution processes but can achieve high power-conversion efficiency (PCE). Many approaches to make efficient solar cells with these perovskite materials have been developed, resulting in an increase of PCE from about 4%[11] to ~20%.[12,13] Enhanced photovoltaic performance of perovskite solar cells toward the Shockley–Quessier limit will benefit to a great extent from an understanding, at the molecular level, of the fundamental photophysical and photochemical processes that occur in these devices, but such an understanding lags much behind the rapid advances in the device fabrication. Although pioneering work using photoluminescence,[14−18] time-resolved microwave conductivity,[17,19,20] and transient absorption[16,18,19] has revealed the nature of charge carriers created in $MAPbX_3$ and their kinetic behavior (in particular on an ultrafast time scale), it is challenging with those methods to observe simultaneously and to identify distinct transient species including not only photogenerated charge carriers but also cations or anions produced as a result of charge transport from the perovskite. This difficulty hampers an elucidation of the relations among the transient species in the same device and thus an understanding of an overall molecular picture of perovskite solar cells.

Time-resolved infrared (IR) spectra provide highly specific information about the molecular structure and dynamics of transient species that is hardly obtainable with macroscopic measurements and electronic spectra. These spectra probe sensitively the photophysical and photochemical reactions that occur on the catalytic metal oxide particles[21,22] and in solutions.[23−27] We applied nanosecond time-resolved IR spectroscopy to study the back electron transfer of pyrene and 1,4-dicyanobenzene in acetonitrile solution and proposed a reaction mechanism in which the solvent plays a significant role as a charge mediator.[28] This preceding work on a simple system in the solution phase has led us to tackle more complicated photovoltaic devices of great importance using nanosecond time-resolved IR spectroscopy.

Here, we report that the time-resolved IR method enables a simultaneous observation of distinct transient species that are formed in $MAPbI_3$ thin films and in $MAPbI_3$ solar cells based on a planar-heterojunction (PHJ) architecture after photoexcitation of the perovskite. Time-resolved IR spectra of a $MAPbI_3$ film recorded in the submicro- to microsecond time regime exhibit broad structureless absorption that is attributable to the intraconduction band transition of photogenerated electrons, together with characteristic dispersive features that result from Fano resonance. When $MAPbI_3$ is incorporated in a

Received: May 23, 2016
Accepted: June 15, 2016
Published: June 15, 2016

DOI: 10.1021/acs.jpclett.6b01111
J. Phys. Chem. Lett. 2016, 7, 2450−2455

PHJ structure with a thin layer of TiO_2 as the hole-blocking material and 2,2′,7,7′-tetrakis(*N*,*N*-di-*p*-methoxyphenylamine)-9,9′-spirobifluorene (spiro-OMeTAD) as the hole-transporting material (HTM), new transient bands appear in the time-resolved IR spectra because of hole transport from the perovskite layer to the HTM layer.[29] The HTM-associated transient species can be assigned to the spiro-OMeTAD cation that decays through charge recombination at the interface between the perovskite and HTM layers. The transient charged species that are observed simultaneously in the present work could provide a quantitative measure of the degree of charge separation, charge transport, and trapping. We underscore both the novel findings obtained and the potential of nanosecond time-resolved IR spectroscopy for fundamental and effective approach to solar cell research.

$MAPbI_3$, with band gap ∼1.6 eV,[1] absorbs almost the entire visible light spectrum (Figure 1a). Two absorption bands

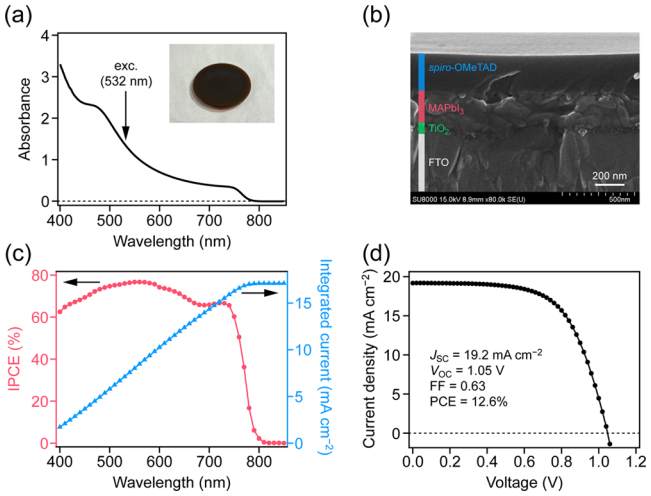

Figure 1. Characterization of perovskite $MAPbI_3$ samples. (a) Electronic absorption spectrum of a $MAPbI_3$ film. The inset shows a photograph of the $MAPbI_3$ film deposited on a CaF_2 substrate for IR measurements. (b) Cross-sectional SEM image of a PHJ perovskite solar cell with device configuration FTO/TiO_2/$MAPbI_3$/spiro-OMeTAD/Ag. Cells fabricated on a FTO substrate were used for the characterization of solar-cell performance but not for IR measurements. Scale bar, 200 nm. (c) IPCE (red circles) and integrated current (blue triangles) spectra of the PHJ device with device architecture FTO/TiO_2/$MAPbI_3$/ spiro-OMeTAD/Ag. (d) Current density−voltage (*J*−*V*) curve of the same device as shown in panel c.

typical of $MAPbI_3$ occur at 480 and 760 nm. In our time-resolved IR experiments presented below, we photoexcited $MAPbI_3$ at 532 nm, which is nearer the 480 nm band.

The PHJ devices tested in this work consisted of a compact TiO_2 underlayer (∼60 nm), a $MAPbI_3$ layer (∼200 nm), a hole-transporting layer of spiro-OMeTAD (∼200 nm), and a silver back contact electrode. Those layers were sequentially deposited on a fluorine-doped tin oxide (FTO) substrate for devices used to characterize photovoltaic performance and on a CaF_2 or BaF_2 substrate (without a silver layer) for samples used in time-resolved IR experiments. Figure 1b shows a cross-sectional scanning electron microscopy (SEM) image of the device fabricated on FTO, revealing that the $MAPbI_3$ in the device was polycrystalline with typical grain size 600−700 nm.

The photovoltaic performance of our device is summarized in Figure 1c,d. Figure 1c displays the incident photon-to-electron conversion efficiency (IPCE) and integrated current spectra; Figure 1d shows the current density versus voltage (*J*−*V*) curve measured under 1 sun illumination (AM1.5G, 100 mW cm^{-2}). The perovskite solar cell showed short-circuit photocurrent (J_{SC}) 19.2 mA cm^{-2}, open-circuit voltage (V_{OC}) 1.05 V, and fill factor (FF) 0.63, yielding overall PCE 12.6%. The performance of our device with an n-i-p PHJ configuration is similar to that of the device made by Xiao et al.[30] with a similar fabrication. The sample preparation and device characterization are described in full detail in the Supporting Information.

We recorded time-resolved IR spectra of a $MAPbI_3$ thin film deposited on BaF_2 excited at 532 nm with laser fluence ∼25 μJ cm^{-2}, using the laboratory-built highly sensitive time-resolved IR spectrometer (see Supporting Information for details of the apparatus).[28,31−33] Unlike the steady-state FTIR spectrum of $MAPbI_3$ (Figure 2a, upper panel), which exhibits several sharp

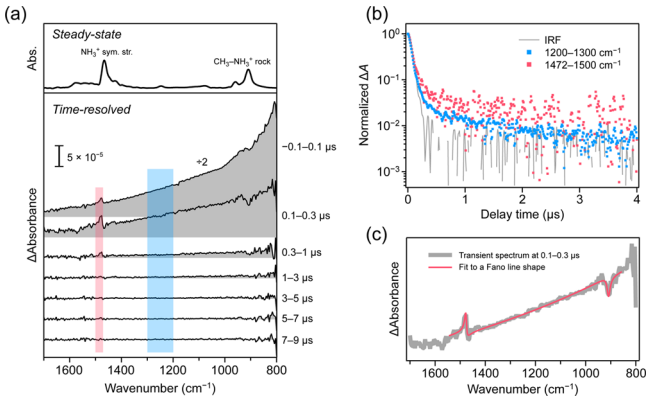

Figure 2. Nanosecond time-resolved IR spectra of a $MAPbI_3$ thin film. (a) Steady-state FTIR spectrum (upper panel) and transient IR spectra (lower panel) of the $MAPbI_3$ film (see the Supporting Information for experimental details). Each time-resolved spectrum is vertically offset by 5 × 10^{-5} for clarity of display. In the time-resolved IR measurement, the sample was rotated at 2000 rpm with a laboratory-built rotor (Figure S1) to avoid possible photochemical damage of the sample and heat accumulation. (b) Logarithmic plot of normalized Δ*A* signals in regions 1200−1300 (blue dots) and 1472−1500 cm^{-1} (red dots) showing decay kinetics. The gray line represents the IRF obtained on measuring scattered laser light. (c) Observed transient IR spectrum at 0.1−0.3 μs (thick gray line) and the best fit to a Fano line shape (red line; see eq S1 in the Supporting Information).

IR bands, the observed transient IR spectra (Figure 2a, lower panel) are dominated by extremely broad and structureless absorption that increases monotonically toward smaller wavenumber; it decays almost completely within a few microseconds. Such a broad transient absorption cannot be due to a vibrational transition and is attributed to the intraband transition of free electrons in the conduction band (CB) of the perovskite. It is well-established that, in semiconductors, free carriers in the CB give rise to a broad IR absorption spectrum that grows toward lower energy.[34] Although Yamakata and co-workers reported similar spectral features in the mid-IR region for platinized TiO_2 particles[21] and La-doped $NaTaO_3$ catalysts,[22] the intraband transition in $MAPbI_3$ perovskite has been directly observed here for the first time.

In addition to the broad intraband transition of CB electrons, we observed dispersive features about 900 and 1480 cm^{-1} with

DOI: 10.1021/acs.jpclett.6b01111
J. Phys. Chem. Lett. 2016, 7, 2450−2455

the negative portion of the dispersive feature on the smaller wavenumber side. As the FTIR spectrum (Figure 2a, upper panel) shows, these wavenumbers correspond to IR bands of the CH_3–NH_3^+ rocking mode and the NH_3^+ symmetric stretching mode of the MA cation, respectively.[35] Each transient feature might thus be interpreted as comprising a transient absorption of some photogenerated MA species (giving the positive signal on the larger wavenumber side) and a depletion of the ground-state population of the MA cation (producing a dip on the smaller wavenumber side). Dispersive spectral features of this type are common when the band of a photogenerated transient such as a molecule in an excited state is blueshifted with respect to the ground-state band, as observed in our previous work.[32] However, the electrons are directly photoexcited in the present experiment, not the MA cation itself. Another effect that might account for the dispersive shapes is that thermal artifacts arise from transient heating of the sample induced by the laser irradiation. Such thermal artifacts typically build up with a delay of hundreds of nanoseconds relative to the photoexcitation and persist for more than 1 μs.[36] Because $MAPbI_3$ polycrystals have been shown to be a poor heat transporter with low thermal conductivity 0.3 $W\,K^{-1}\,m^{-1}$,[37] the decay of the thermal artifacts would not be much faster than ~1 μs. We therefore exclude a possibility that the present transient dispersive features are due primarily to this source.

What then is the origin of the dispersive features? We propose to attribute them to Fano resonances between the vibrational transitions of the MA cation and the quasi-continuous intra-CB transition. A Fano resonance occurs when there are a discrete state and a continuum in the system that are resonantly coupled to each other;[38] a dispersive line shape depends on asymmetry parameter q. This assignment is corroborated on comparing the temporal profiles in regions 1200–1300 cm^{-1} (the intraband absorption signal) and 1472–1500 cm^{-1} (the positive portion of the dispersive feature) (Figure 2b). Both profiles exhibit similar rapid [limited according to the instrumental response function (IRF)] and slow decay components, strongly indicating that the dispersive features observed in the IR bands of the MA cation are correlated with the intraband transition. This correlation disfavors an assignment of the dispersive features to structural changes of $MAPbI_3$.[10,39] Another support for our hypothesis comes from the fact that the dispersive features about 900 and 1480 cm^{-1} are well fitted with a theoretical formula for Fano line shapes (eq S1),[40,41] as shown in Figure 2c. The fitting parameters so obtained, including q, are all fairly reasonable (see Table S1).

The decay of the transient IR signals (both the intraband transition and Fano-resonance features) reflects charge recombination, as depicted in Figure 3. The rapid decay component cannot be resolved in the present experiments because the temporal resolution of our apparatus is ~80 ns. This result is consistent with the reported time constants of the photoluminescence and transient absorption decays (of order 10 ns; refs 15–18). A tiny but finite fraction of photogenerated carriers might be trapped in the subgap states (see Figure 3). Because this trapping occurs on a picosecond time regime,[42] its observation was impracticable. What we could see is the subsequent recombination of trapped carriers. Trapped electrons would undergo slower, nongeminate recombination, which might account for the slow decay component observed in Figure 2b. The direct transition of trapped electrons to the

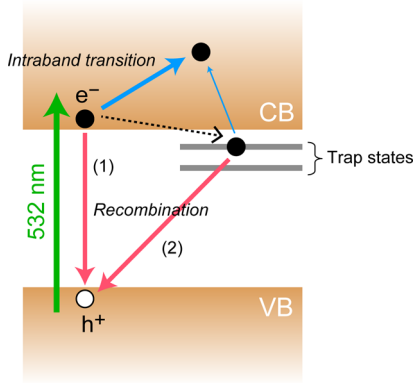

Figure 3. Schematic to illustrate optical and physical processes. After photoexcitation at 532 nm, photogenerated electrons recombine with holes via two channels: (1) they undergo direct recombination, and (2) they are first trapped in the subgap states (trap states) after which the resulting trapped electrons recombine with holes. These recombination processes together are responsible for the decay of the transient IR signal (see Figure 2).

CB might overlap the broad intra-CB transition.[21] However, its contribution is expected to be minor because the amplitude of the slow decay component is much smaller than that of the rapid decay component (see Figure 2b).

Next, we present the transient IR spectra of a TiO_2/$MAPbI_3$/spiro-OMeTAD film corresponding to the PHJ device (Figure 4a, lower panel). Whereas BaF_2 was used for $MAPbI_3$ thin films,

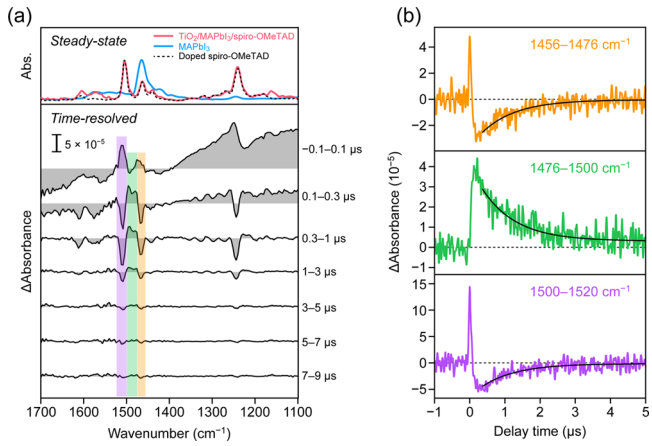

Figure 4. Nanosecond time-resolved IR spectra of a TiO_2/$MAPbI_3$/spiro-OMeTAD film. (a) Steady-state FTIR spectra of the TiO_2/$MAPbI_3$/spiro-OMeTAD film (red trace, upper panel), $MAPbI_3$ (blue trace, upper panel), and doped spiro-OMeTAD (black dashed trace, upper panel) and transient IR spectra of the TiO_2/$MAPbI_3$/spiro-OMeTAD film (lower panel). Each time-resolved spectrum is vertically offset by 1×10^{-4} for clarity of display. (b) Temporal evolution of the integrated ΔA signal in regions 1456–1476 cm^{-1} (yellow trace, top panel), 1476–1500 cm^{-1} (green trace, middle panel), and 1500–1520 cm^{-1} (purple trace, bottom panel). The black lines are fits to an exponential function with time constant 1.0 μs.

the PHJ layers were prepared on a CaF_2 substrate because of the annealing temperature required for TiO_2. The transient IR spectra in Figure 4a are consequently confined to the 1100–1700 cm^{-1} range, narrower than those in Figure 2a. As is the case for $MAPbI_3$ thin films, we found broad absorption that is attributed to an intraband transition of CB electrons. In the sample TiO_2/$MAPbI_3$/spiro-OMeTAD, a broad negative

DOI: 10.1021/acs.jpclett.6b01111
J. Phys. Chem. Lett. 2016, 7, 2450–2455

feature was additionally observed above ~1520 cm^{-1}. A similar negative feature was found for the $MAPbI_3$ film, but at greater wavenumber (Figure S2). This signal does not represent a depletion of absorption because there is no corresponding IR absorption of the sample that extends above 1600 cm^{-1} (see the steady-state FTIR spectrum of the $TiO_2/MAPbI_3$/spiro-OMeTAD film shown in Figure 4a, upper panel). Our preliminary experiments show that the negative feature is not due to spontaneous emission (photoluminescence) and, furthermore, that it is significantly sample-dependent. To the best of our knowledge, emission extending from the mid-IR has not been reported for these perovskites. Clarification of the origin of the "emission-like" signal is left for future studies in both mid- and near-IR regions.

We now focus on the vibrational features observed at ~1240 cm^{-1} and between 1450−1520 cm^{-1}; those features were not at all observed in the $MAPbI_3/TiO_2$ film (Figure S3), indicating that they originate from spiro-OMeTAD with a p-dopant. The positive features that are prominent at brief delays (see, for example, the −0.1 to 0.1 μs spectrum in Figure 4a) may again be attributed to the Fano effect, but in this case it should be the intermolecular Fano resonance between $MAPbI_3$ and spiro-OMeTAD. A similar phenomenon involving intermolecular mixing of discrete and continuous states has previously been reported on CO adsorbed on Cu[43] and organic solvent molecules on TiO_2 nanoparticles.[44] The transient bands at ~1240 cm^{-1} and between 1450−1520 cm^{-1} rapidly disappear within the temporal resolution of our apparatus, leaving the negative signals at nearly the same wavenumbers. The negative signals at ~1240, 1465, and 1510 cm^{-1}, at which doped spiro-OMeTAD has intense IR bands (see the FTIR spectrum (dashed line) in Figure 4a, upper panel), represent the depletion of doped spiro-OMeTAD. The doped spiro-OMeTAD represents mainly the neutral species but might have a minor contribution from the cation. As opposed to the MA cation (see above), spiro-OMeTAD can be depleted even though it shows only negligible absorption at 532 nm,[45,46] because hole migration from the perovskite layer to the HTM layer leads to the formation of the spiro-OMeTAD cation and a concomitantly decreased population of the neutral species in the doped spiro-OMeTAD. Between the depletion at 1465 and 1510 cm^{-1} lie new transient absorption signals that were observed in the steady-state IR spectra of neither spiro-OMeTAD nor $MAPbI_3$; these bands and the depletion signals appear to decay in unison.

To examine the kinetics of the transients and to obtain clues about the transient absorption about 1485 cm^{-1}, we compare the temporal profiles of the integrated ΔA signals in regions 1456−1476, 1476−1500, and 1500−1520 cm^{-1} in Figure 4b. The temporal profiles of the depletion signals at 1465 and 1510 cm^{-1}, shown in Figure 4b as yellow (top) and purple (bottom) traces, respectively, exhibit an IRF-limited spike, followed by a slow recovery that reflects the regeneration of neutral spiro-OMeTAD from its cationic form. In contrast, the temporal profile at ~1485 cm^{-1} [Figure 4b, green (middle) trace] comprises an initial rapid rise (IRF-limited) and a subsequent slow decay due to charge recombination. The slow decay after ~400 ns of the three temporal profiles can all be fitted satisfactorily with an exponential function and time constant τ = 1.0 (±0.2) μs (Figure 4b, black lines). This result seems to indicate that the transient absorption signals in region 1476−1500 cm^{-1} are associated with the spiro-OMeTAD cation (HTM^+), but the lifetime of the spiro-OMeTAD cation on a mesoporous $TiO_2/MAPbI_3$/spiro-OMeTAD sample probed in the near-IR region (λ = 1.4 μm) with laser fluence higher (70 $\mu J\ cm^{-2}$) than ours (25 $\mu J\ cm^{-2}$) was reported to be ~100 μs.[19] Tachibana and co-workers monitored the spiro-OMeTAD cation at 1.6 μm with laser fluecne 120 $\mu J\ cm^{-2}$, which exhibited even slower recombination.[47] These results contradict the kinetics observed in the mid-IR region (λ = 6.7 μm). We therefore interpret the transient species at ~1485 cm^{-1} as the spiro-OMeTAD cation that specifically reflects charge recombination at the interface between perovskite and spiro-OMeTAD. After charge separation in $MAPbI_3$, electrons and holes diffuse across the perovskite layer toward TiO_2 and spiro-OMeTAD, respectively. Electron and hole injections occur on time scales that are much smaller than the response of our detection system.[19,47] The holes injected into the HTM layer oxidize spiro-OMeTAD. We propose that a loss of a portion of the resulting cationic species occurs as holes recombine with electrons in $MAPbI_3$ (rather than those in TiO_2) at the perovskite/spiro-OMeTAD interface, at which free or trapped electrons are available for rapid recombination to occur, and hence has a substantially smaller lifetime (~1 μs) than the reported value (~100 μs). The above scenario is schematically illustrated in Figure 5.

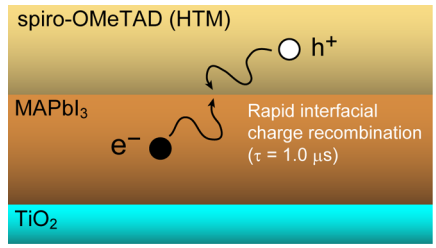

Figure 5. Schematic representation of charge recombination at the interface between the perovskite and spiro-OMeTAD. This process occurs with time constant τ = 1.0 μs, which is much smaller than the reported value (~100 μs) for a mesoporous $TiO_2/MAPbI_3$/spiro-OMeTAD sample.[19]

In conclusion, we have observed simultaneously in the transient IR spectra (i) CB electrons in $MAPbI_3$ (manifested as a broad intraband absorption), (ii) neutral spiro-OMeTAD (depletion bands), and (iii) the spiro-OMeTAD cation that is associated with interfacial charge recombination (transient absorption about 1485 cm^{-1}). This capability of simultaneous observation is noteworthy. Most prior authors employed other spectroscopic methods to characterize transient species individually,[19,20] making it difficult to compare directly the results and to regard the interplay among them in a comprehensive manner. Here, we summarize the implications of the three transient species to characterize perovskite solar cells as follows.

(1) The maximum absorption intensity of CB electrons could provide a quantitative measure of the efficiency of charge separation induced in the perovskite: the greater the intensity, the more charge carriers are generated.

(2) The amplitudes of the depletion signals of doped spiro-OMeTAD are proportional to the concentration of the spiro-OMeTAD cation that is formed as a result of hole transport to the HTM. By monitoring the depletion signals at 1240, 1465, and 1510 cm^{-1}, we can know the extent of hole transport to the spiro-OMeTAD layer.

DOI: 10.1021/acs.jpclett.6b01111
J. Phys. Chem. Lett. 2016, 7, 2450−2455

(3) The spiro-OMeTAD cation that has lifetime 1.0 μs could provide insight into the nature of the charge recombination at the perovskite/spiro-OMeTAD interface. Because its amplitude and lifetime are expected to be affected strongly by the interface morphology, the information that the present work provides would help to develop novel methods to prepare the perovskite/spiro-OMeTAD interface with improved hole transport.

Unlike photovoltaic characterization such as $J-V$ curve measurements, the insights gained with time-resolved IR spectroscopy are highly specific to individual molecular species that play a crucial role in different fundamental processes inside the device (charge separation, transport, and/or recombination) and hence will enable one to devise an efficient strategy to further improve the device performance. This approach based on the molecular-level understanding of perovskite solar cells is complementary to the systematic approach often undertaken in materials science.

In addition to the transient species summarized above, we highlight the novel finding of Fano-resonance features that involve the CB continuum of the perovskite and vibrational transitions of the perovskite or spiro-OMeTAD. The present method is readily applicable to perovskite solar cells using other electron-transporting and hole-transporting materials with either mesoporous or planar architectures. It will therefore be a valuable asset in further enhancing the performance of perovskite solar cells based on a basic understanding of the underlying photophysical and photochemical processes.

■ ASSOCIATED CONTENT

Supporting Information

The Supporting Information is available free of charge on the ACS Publications website at DOI: 10.1021/acs.jpclett.6b01111.

Experimental methods, schematics of the sample rotor, time-resolved near-IR spectra of a $MAPbI_3$ film, and time-resolved IR spectra of a $TiO_2/MAPbI_3$ film (PDF)

■ AUTHOR INFORMATION

Corresponding Authors

*E-mail: diau@mail.nctu.edu.tw.

*E-mail: shigeto@kwansei.ac.jp.

Notes

The authors declare no competing financial interest.

■ ACKNOWLEDGMENTS

We thank Liang-Cheng Kuo for his contribution to the design of the sample rotor and for measuring time-resolved near-IR spectra of the perovskite film. Ministry of Education, Taiwan; National Chiao Tung University ("Aiming for the Top University" program); and Ministry of Science and Technology, Taiwan (Grants MOST103-2745-M-009-001-ASP, MOST103-2923-M-009-005-MY2, and MOST102-2113-M-009-020-MY3) provided financial support.

■ REFERENCES

(1) Lee, M. M.; Teuscher, J.; Miyasaka, T.; Murakami, T. N.; Snaith, H. J. Efficient Hybrid Solar Cells Based on Meso-Superstructured Organometal Halide Perovskites. *Science* **2012**, *338*, 643−647.

(2) Burschka, J.; Pellet, N.; Moon, S.-J.; Humphry-Baker, R.; Gao, P.; Nazeeruddin, M. K.; Grätzel, M. Sequential Deposition as a Route to High-Performance Perovskite-Sensitized Solar Cells. *Nature* **2013**, *499*, 316−319.

(3) Liu, M.; Johnston, M. B.; Snaith, H. J. Efficient Planar Heterojunction Perovskite Solar Cells by Vapor Deposition. *Nature* **2013**, *501*, 395−398.

(4) Park, N.-G. Organometal Perovskite Light Absorers toward a 20% Efficiency Low-Cost Solid-State Mesoscopic Solar Cell. *J. Phys. Chem. Lett.* **2013**, *4*, 2423−2429.

(5) Snaith, H. J. Perovskites: The Emergence of a New Era for Low-Cost, High-Efficiency Solar Cells. *J. Phys. Chem. Lett.* **2013**, *4*, 3623−3630.

(6) Christians, J. A.; Manser, J. S.; Kamat, P. V. Multifaceted Excited State of $CH_3NH_3PbI_3$. Charge Separation, Recombination, and Trapping. *J. Phys. Chem. Lett.* **2015**, *6*, 2086−2095.

(7) Eames, C.; Frost, J. M.; Barnes, P. R. F.; O'Regan, B. C.; Walsh, A.; Islam, M. S. Ionic Transport in Hybrid Lead Iodide Perovskite Solar Cells. *Nat. Commun.* **2015**, *6*, 7497.

(8) Leguy, A. M. A.; Frost, J. M.; McMahon, A. P.; Sakai, V. G.; Kochelmann, W.; Law, C.; Li, X.; Foglia, F.; Walsh, A.; O'Regan, B. C.; et al. The Dynamics of Methylammonium Ions in Hybrid Organic-Inorganic Perovskite Solar Cells. *Nat. Commun.* **2015**, *6*, 7124.

(9) Park, B.-w.; Jain, S. M.; Zhang, X.; Hagfeldt, A.; Boschloo, G.; Edvinsson, T. Resonance Raman and Excitation Energy Dependent Charge Transfer Mechanism in Halide-Substituted Hybrid Perovskite Solar Cells. *ACS Nano* **2015**, *9*, 2088−2101.

(10) Quarti, C.; Mosconi, E.; Ball, J. M.; D'Innocenzo, V.; Tao, C.; Pathak, S.; Snaith, H. J.; Petrozza, A.; De Angelis, F. Structural and Optical Properties of Methylammonium Lead Iodide across the Tetragonal to Cubic Phase Transition: Implications for Perovskite Solar Cells. *Energy Environ. Sci.* **2016**, *9*, 155−163.

(11) Kojima, A.; Teshima, K.; Shirai, Y.; Miyasaka, T. Organometal Halide Perovskites as Visible-Light Sensitizers for Photovoltaic Cells. *J. Am. Chem. Soc.* **2009**, *131*, 6050−6051.

(12) Zhou, H.; Chen, Q.; Li, G.; Luo, S.; Song, T.-b.; Duan, H.-S.; Hong, Z.; You, J.; Liu, Y.; Yang, Y. Interface Engineering of Highly Efficient Perovskite Solar Cells. *Science* **2014**, *345*, 542−546.

(13) Yang, H. S.; Noh, J. H.; Jeon, N. J.; Kim, Y. C.; Ryu, S.; Seo, J.; Seok, S. I. High-Performance Photovoltaic Perovskite Layers Fabricated through Intramolecular Exchange. *Science* **2015**, *348*, 1234−1237.

(14) Stranks, S. D.; Burlakov, V. M.; Leijtens, T.; Ball, J. M.; Goriely, A.; Snaith, H. J. Recombination Kinetics in Organic-Inorganic Perovskites: Excitons, Free Charge, and Subgap States. *Phys. Rev. Appl.* **2014**, *2*, 034007.

(15) Hsu, H.-Y.; Wang, C.-Y.; Fathi, A.; Shiu, J.-W.; Chung, C.-C.; Shen, P.-S.; Guo, T.-F.; Chen, P.; Lee, Y.-P.; Diau, E. W.-G. Femtosecond Excitonic Relaxation Dynamics of Perovskite on Mesoporous Films of Al_2O_3 and NiO Nanoparticles. *Angew. Chem., Int. Ed.* **2014**, *53*, 9339−9342.

(16) Yamada, Y.; Nakamura, T.; Endo, M.; Wakamiya, A.; Kanemitsu, Y. Photocarrier Recombination Dynamics in Perovskite $CH_3NH_3PbI_3$ for Solar Cell Applications. *J. Am. Chem. Soc.* **2014**, *136*, 11610−11613.

(17) Hutter, E. M.; Eperon, G. E.; Stranks, S. D.; Savenije, T. J. Charge Carrier in Planar and Meso-Structured Organic-Inorganic Perovskites: Mobilities, Lifetimes, and Concentrations of Trap States. *J. Phys. Chem. Lett.* **2015**, *6*, 3082−3090.

(18) Shi, D.; Adinolfi, V.; Comin, R.; Yuan, M.; Alarousu, E.; Buin, A.; Chen, Y.; Hoogland, S.; Rothenberger, A.; Katsiev, K.; et al. Low Trap-State Density and Long Carrier Diffusion in Organolead Trihalide Perovskite Single Crystals. *Science* **2015**, *347*, 519−522.

(19) Marchioro, A.; Teuscher, J.; Friedrich, D.; Kunst, M.; van de Krol, R.; Moehl, T.; Grätzel, M.; Moser, J.-E. Unravelling the Mechanism of Photoinduced Charge Transfer Processes in Lead Iodide Perovskite Solar Cells. *Nat. Photonics* **2014**, *8*, 250−255.

(20) Ponseca, C. S., Jr.; Savenije, T. J.; Abdellah, M.; Zheng, K.; Yartsev, A.; Pascher, T.; Harlang, T.; Chabera, P.; Pullerits, T.; Stepanov, A.; et al. Organometal Halide Perovskite Solar Cell Materials Rationalized: Ultrafast Charge Generation, High and Microsecond-Long Balanced Mobilities, and Slow Recombination. *J. Am. Chem. Soc.* **2014**, *136*, 5189−5192.

DOI: 10.1021/acs.jpclett.6b01111
J. Phys. Chem. Lett. 2016, 7, 2450−2455

(21) Yamakata, A.; Ishibashi, T.; Onishi, H. Time-Resolved Infrared Absorption Spectroscopy of Photogenerated Electrons in Platinized TiO_2 Particles. *Chem. Phys. Lett.* **2001**, *333*, 271−277.
(22) Yamakata, A.; Ishibashi, T.; Kato, H.; Kudo, A.; Onishi, H. Photodynamics of $NaTaO_3$ Catalysts for Efficient Water Splitting. *J. Phys. Chem. B* **2003**, *107*, 14383−11387.
(23) Yuzawa, T.; Hamaguchi, H. Investigation of the Photoisomerization of All-*trans*-Retinal by Singular-Value-Decomposition Analysis of Nanosecond Time-Resolved Infrared Spectra. *J. Mol. Struct.* **1995**, *352-353*, 489−495.
(24) Bridgewater, J. S.; Lee, B.; Bernhard, S.; Schoonover, J. R.; Ford, P. C. Time-Resolved Infrared Spectral Studies of Photochemically Induced Oxidative Addition of Benzene to *trans*-RhCl(CO) $(PMe_3)_2$. *Organometallics* **1997**, *16*, 5592−5594.
(25) Kwok, W.-M.; George, M. W.; Grills, D. C.; Ma, C.; Matousek, P.; Parker, A. W.; Phillips, D.; Toner, W. T.; Towrie, M. Direct Observation of a Hydrogen-Bonded Charge-Transfer State of 4-Dimethylaminobenzonitrile in Methanol by Time-Resolved IR Spectroscopy. *Angew. Chem., Int. Ed.* **2003**, *42*, 1826−1830.
(26) Yabumoto, S.; Sato, S.; Hamaguchi, H. Vibrational and Electronic Infrared Absorption Spectra of Benzophenone in the Lowest Excited Triplet State. *Chem. Phys. Lett.* **2005**, *416*, 100−103.
(27) Zou, X.; Dai, X.; Liu, K.; Zhao, H.; Song, D.; Su, H. Photophysical and Photochemical Properties of 4-Thiouracil: Time-Resolved IR Spectroscopy and DFT Studies. *J. Phys. Chem. B* **2014**, *118*, 5864−5872.
(28) Narra, S.; Nishimura, Y.; Witek, H. A.; Shigeto, S. Mechanism of Back Electron Transfer in an Intermolecular Photoinduced Electron Transfer Reaction: Solvent as a Charge Mediator. *ChemPhysChem* **2014**, *15*, 2945−2950.
(29) Brauer, J. C.; Lee, Y. H.; Nazeeruddin, M. K.; Banerji, N. Charge Transfer Dynamics from Organometal Halide Perovskite to Polymeric Hole Transport Materials in Hybrid Solar Cells. *J. Phys. Chem. Lett.* **2015**, *6*, 3675−3681.
(30) Xiao, M.; Huang, F.; Huang, W.; Dkhissi, Y.; Zhu, Y.; Etheridge, J.; Gray-Weale, A.; Bach, U.; Cheng, Y.-B.; Spiccia, L. A Fast Deposition-Crystallization Procedure for Highly Efficient Lead Iodide Perovskite Thin-Film Solar Cells. *Angew. Chem., Int. Ed.* **2014**, *53*, 9898−9903.
(31) Yabumoto, S.; Shigeto, S.; Lee, Y.-P.; Hamaguchi, H. Ordering, Interaction, and Reactivity of the Low-Lying $n\pi^*$ and $\pi\pi^*$ Excited Triplet States of Acetophenone Derivatives. *Angew. Chem., Int. Ed.* **2010**, *49*, 9201−9205.
(32) Narra, S.; Chang, S.-W.; Witek, H. A.; Shigeto, S. Is Our Way of Thinking About Excited States Correct? Time-Resolved Dispersive IR Study on *p*-Nitroaniline. *Chem. - Eur. J.* **2012**, *18*, 2543−2550.
(33) Narra, S.; Shigeto, S. Direct Observation of the Solvent Effects on the Low-Lying $n\pi^*$ and $\pi\pi^*$ Excited Triplet States of Acetophenone Derivatives in Thermal Equilibrium. *J. Phys. Chem. B* **2015**, *119*, 3808−3814.
(34) Pankove, J. I. *Optical Processes in Semiconductors*; Dover: New York, 1971.
(35) Glaser, T.; Müller, C.; Sendner, M.; Krekeler, C.; Semonin, O. E.; Hull, T. D.; Yaffe, O.; Owen, J. S.; Kowalsky, W.; Pucci, A.; et al. Infrared Spectroscopic Study of Vibrational Modes in Methylammonium Lead Halide Perovskites. *J. Phys. Chem. Lett.* **2015**, *6*, 2913−2918.
(36) Yuzawa, T.; Kato, C.; George, M. W.; Hamaguchi, H. Nanosecond Time-Resolved Infrared Spectroscopy with a Dispersive Scanning Spectrometer. *Appl. Spectrosc.* **1994**, *48*, 684−690.
(37) Pisoni, A.; Jaćimović, J.; Barišić, O. S.; Spina, M.; Gaál, R.; Forró, L.; Horváth, E. Ultra-Low Thermal Conductivity in Organic-Inorganic Hybrid Perovskite $CH_3NH_3PbI_3$. *J. Phys. Chem. Lett.* **2014**, *5*, 2488−2492.
(38) Fano, U. Effects of Configuration Interaction on Intensities and Phase Shifts. *Phys. Rev.* **1961**, *124*, 1866−1878.
(39) Gottesman, R.; Gouda, L.; Kalanoor, B. S.; Haltzi, E.; Tirosh, S.; Rosh-Hodesh, E.; Tischler, Y.; Zaban, A.; Quarti, C.; Mosconi, E.; et al. Photoinduced Reversible Structural Transformations in Free-Standing $CH_3NH_3PbI_3$ Perovskite Films. *J. Phys. Chem. Lett.* **2015**, *6*, 2332−2338.
(40) Rousseau, D. L.; Porto, S. P. S. Auger-Like Resonant Interference in Raman Scattering from One- and Two-Photon States of $BaTiO_3$. *Phys. Rev. Lett.* **1968**, *20*, 1354−1357.
(41) Blinc, R.; Ferraro, J. R.; Postmus, C. Effects of High Pressure on the Far-Infrared Spectra of Paraelectric KH_2PO_4 and RbH_2PO_4. *J. Chem. Phys.* **1969**, *51*, 732.
(42) Wu, X.; Trinh, M. T.; Niesner, D.; Zhu, H.; Norman, Z.; Owen, J. S.; Yaffe, O.; Kudisch, B. J.; Zhu, X.-Y. Trap States in Lead Iodide Perovskites. *J. Am. Chem. Soc.* **2015**, *137*, 2089−2096.
(43) Hirschmugl, C. J.; Williams, G. P.; Hoffmann, F. M.; Chabal, Y. J. Adsorbate-Substrate Resonant Interactions Observed for CO on Cu(100) in the Far Infrared. *Phys. Rev. Lett.* **1990**, *65*, 480−483.
(44) Matsuzaki, K.; Shimada, R.; Hamaguchi, H. Detection of Solvent/Buried TiO_2 Surface Interactions by Intermolecular Fano Resonance in Resonance Hyper-Raman Scattering. *Langmuir* **2013**, *29*, 2471−2475.
(45) Wang, S.; Yuan, W.; Meng, Y. S. Spectrum-Dependent Spiro-OMeTAD Oxidization Mechanism in Perovskite Solar Cells. *ACS Appl. Mater. Interfaces* **2015**, *7*, 24791−24798.
(46) Fantacci, S.; De Angelis, F.; Nazeeruddin, M. K.; Grätzel, M. Electronic and Optical Properties of the Spiro-MeOTAD Hole Conductor in Its Neutral and Oxidized Forms: A DFT/TDDFT Investigation. *J. Phys. Chem. C* **2011**, *115*, 23126−23133.
(47) Makuta, S.; Liu, M.; Endo, M.; Nishimura, H.; Wakamiya, A.; Tachibana, Y. Photo-Excitation Intensity Dependent Electron and Hole Injections from Lead Iodide Perovskite to Nanocrystalline TiO_2 and Spiro-OMeTAD. *Chem. Commun.* **2016**, *52*, 673−676.

DOI: 10.1021/acs.jpclett.6b01111
J. Phys. Chem. Lett. 2016, 7, 2450−2455